LANGMUIR Article
Cite This: Langmuir 2018, 34, 4132–4141
pubs.acs.org/Langmuir

# Flexible Ultraviolet and Ambient Light Sensor Based on a Nanomaterial Network Fabricated Using Selective and Localized Wet Chemical Reactions

Daejong Yang,[†,‡,§] Jaehwan Lee,[†,‡] Donghwan Kim,[†,‡] Incheol Cho,[†,‡] Jong G. Ok,[∥] and Inkyu Park*[,†,‡]

[†]Department of Mechanical Engineering and [‡]KI for the NanoCentury, Korea Advanced Institute of Science and Technology (KAIST), Daejeon 34141, South Korea

[§]Department of Medical Engineering, California Institute of Technology, Pasadena, California 91125, United States

[∥]Department of Mechanical and Automotive Engineering, Seoul National University of Science and Technology, Seoul 01811, South Korea

Supporting Information

**ABSTRACT:** We report ZnO nanowire- and $TiO_2$ nanotube-based light sensors on flexible polymer substrates fabricated by localized hydrothermal synthesis and liquid phase deposition (LPD). This method realized simple and cost-effective in situ synthesis and integration of one-dimensional ZnO and $TiO_2$ nanomaterials. The fabricated sensor devices with ZnO nanowires and $TiO_2$ nanotubes show very high sensitivity and quick response to the ultraviolet (UV) and ambient light, respectively. In addition, our direct synthesis and integration method result in mechanical robustness under external loading such as static and cyclic bending because of the strong bonding between the nanomaterial and the electrode. By controlling the reaction time of the LPD process, the Ti/Zn ratio could be simply modulated and the spectral sensitivity to the light in the UV to visible range could be controlled.

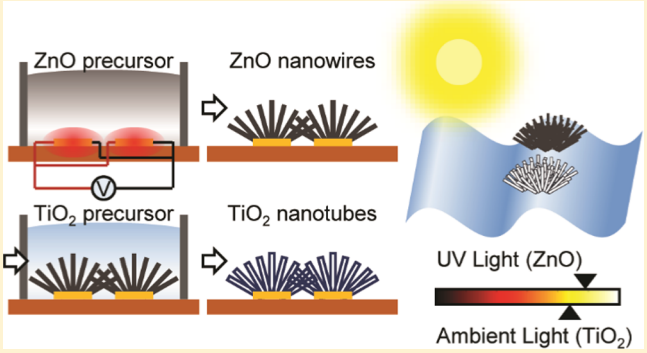


## INTRODUCTION

One-dimensional (1D) nanomaterials such as nanowires and nanotubes have attracted a great deal of attention because of their novel properties and versatile applications, such as field effect transistor,[1] energy generation,[2,3] energy storage,[4] field emission,[5] and physical/chemical sensing.[6−8] Especially, they have shown great potentials for sensing applications because of their unique physical and chemical properties such as high crystallinity,[9,10] versatile chemical compositions,[11] tunable band gap,[12,13] chemical reactivity,[14] small dimension, and high surface-to-volume ratio.[15,16] Because of these advantages, many 1D nanomaterial sensors have been widely developed.[17−19] In particular, ZnO is an n-type semiconductor material with a wide direct band gap energy of 3.37 eV and large exciton binding energy of 60 meV, which make it an outstanding material for photonic sensing in the UV range.[20] Bai, et al.[21] fabricated ZnO nanowire-based UV photodetectors with ultrahigh sensitivity ($I/I_0 > 10^5$). In addition, Alenezi, et al.[22] made ultrafast ($\tau$ < 100 ms) ZnO nanowire-based UV photodetectors.

Especially in electrical device applications, 1D nanomaterials have to be assembled and integrated on device electrodes in the electrical circuit. The most common method to connect 1D nanomaterials and electrodes is drop casting of nanomaterial solution onto the electrodes.[23] Although this is a very simple and cost-effective integration method, it only produces randomly dispersed nanowire networks and provides limited patterning resolution (minimum diameter ∼1 mm) and thus is not suitable for highly integrated, ultracompact devices.[24,25] For more accurate and delicate device integration of 1D nanomaterials, numerous methods such as screen printing,[26,27] inkjet printing,[28] contact printing,[21,29] optical trapping,[30] atomic force microscopy (AFM),[31] electrostatic force,[32] magnetic force,[33] and dielectrophoresis[34] have been utilized. The printing methods such as screen printing and inkjet printing are simple but provide limited resolutions (minimum diameter ∼100 $\mu$m). Optical trapping and AFM-based methods provide much higher integration accuracy but require expensive equipment and allow limited throughput. Because the methods based on magnetic, electrostatic, or dielectrophoretic force use liquid suspension of nanomaterials, deposition of nanomaterials can occur at undesired locations via nonselective physical adsorption. Moreover, abovementioned methods provide only the alignment and placement of nanomaterials, not the reliable bonding

Received: July 5, 2017
Revised: January 7, 2018
Published: March 14, 2018






DOI: 10.1021/acs.langmuir.7b02332
Langmuir 2018, 34, 4132−4141

between nanomaterials and electrodes, and therefore mechanical robustness cannot be guaranteed.

To solve these technical issues of controlled and reliable integration of 1D nanomaterials for the fabrication of highly integrated sensors, we have developed a novel and facile method for the in situ synthesis and integration in selected locations using sequential localized liquid-phase reactions.[18,35] The fabrication processes have been specially designed for flexible substrates to widen the application of this method. In addition, numerical analysis on flexible substrates has also been discussed in detail. As shown in Figure 1, the microheater

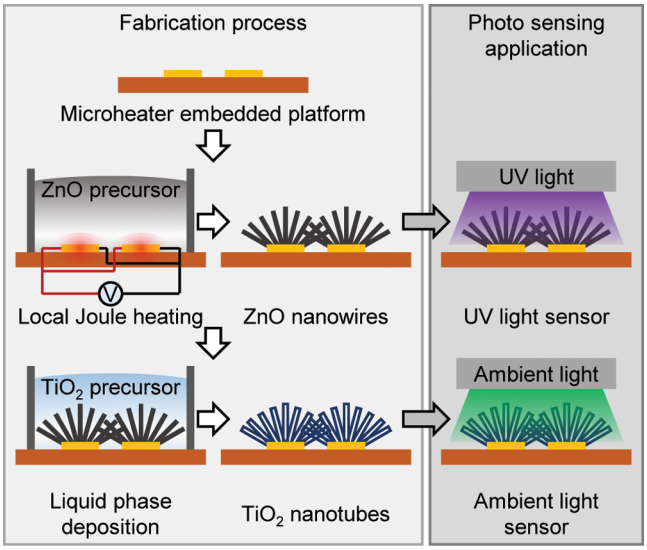


**Figure 1.** Schematic of the process flow for the ZnO nanowire and $TiO_2$ nanotube synthesis. ZnO nanowires are synthesized by the local hydrothermal reaction along microheaters, and presynthesized ZnO nanowires are converted to $TiO_2$ nanotubes by liquid phase deposition (LPD).

generates a local hot spot by Joule heating and nanowires are synthesized on the surface of the microheater. The local heating induces convective flow of precursor solution and enables continuous and localized synthesis of the nanowires. In this work, we applied this method to the synthesis of ZnO nanowires. After the synthesis of ZnO nanowires, they were converted to $TiO_2$ nanotubes by room temperature liquid-phase reaction within $TiO_2$ precursor solution. Because these reactions occur at a very low temperature (<100 °C) and use mild and noncorrosive chemicals, nanomaterials can also be directly synthesized on flexible polymer substrates. The most significant advantages of this method are (1) direct synthesis and integration of nanomaterials without the requirement of further assembly and integration processes, (2) simple and low-cost setup for the process, (3) operation under low-temperature, liquid, and atmospheric pressure conditions, and (4) mechanically and electrically robust bonding between synthesized nanomaterials and electrodes. All of these advantages can serve as essential factors for the application to flexible electronic devices.

## MATERIALS AND METHODS

**Fabrication of the Microheater Platform.** Polyimide (PI, 75 $\mu$m thick, PIF075, Shinmax Technology Ltd., Taiwan) was used as the substrate for the fabrication of a flexible light sensor. The microheaters were fabricated using conventional photolithography and metal lift-off processes. The photoresist (AZ9260, MicroChemicals GmbH, Germany) was first coated on the silicon (Si) wafer, and the polyimide (PI) film was attached on the Si wafer using the spin-coated photoresist as a temporary adhesive. The photoresist (AZ5214, MicroChemicals GmbH, Germany) was patterned for microheaters and pads on the PI film using the photolithography process. Chrome (Cr, 10 nm thick) was deposited as the adhesion layer, and a gold (Au, 200 nm thick) film was also deposited on the substrate by electron beam evaporation. The substrate was immersed in acetone to remove the photoresist pattern and dummy Cr/Au film. Finally, the PI film was separated from the Si wafer.

**Synthesis of ZnO Nanowires.** Two methanol-based solutions consisting of 10 mM zinc acetate dihydrate ($Zn(CH_3COO)_2{\cdot}2H_2O$) and 30 mM potassium hydroxide (KOH) were prepared and heated to 60 °C. The volumetric ratio of the former to the latter was 25:13. The KOH solution was added dropwise to the zinc acetate dihydrate solution while maintaining the temperature. The mixture was stirred for 2 h at 60 °C.[36] The microheater platforms were coated with the ZnO nanoparticle solution and heated to 150 °C on a hotplate for 20 min. Zinc nitrate hydrate ($Zn(NO_3)_2{\cdot}6H_2O$, 25 mM), hexamethylenetetramine ($C_6H_{12}N_4$, 25 mM), and polyethylenimine ($(C_2H_5N)_n$, 6 mM) were mixed in the deionized (DI) water as the precursor solution for the ZnO nanowire synthesis (all chemicals were purchased from Sigma-Aldrich). A small polydimethylsiloxane (PDMS) well was attached on the microheater device and filled with 10 $\mu$L of the ZnO nanowire precursor solution. A direct current (DC) bias of 0.28 V was applied to the microheaters for 30 min for Joule heating. The whole synthesis process was monitored in real time by a high-resolution optical microscope (BX51M, Olympus, Japan).

**Synthesis of $TiO_2$ Nanotubes.** The precursor solution consisting of 0.3 M boric acid ($H_3BO_3$) and 0.1 M ammonium hexafluorotitanate ($(NH_4)_2TiF_6$) in DI water was prepared for the synthesis of $TiO_2$ nanotubes (all chemicals were purchased from Sigma-Aldrich). A PDMS well was attached on the microheater device with presynthesized ZnO nanowires, and 10 $\mu$L of $TiO_2$ precursor solution was supplied for 15 min at room temperature with no additional heating.

**Optical Characterization of the ZnO–$TiO_2$ Nanocomposite.** ZnO nanowires were synthesized on a cover glass (Cover Slips (22 mm × 22 mm), Duran Group, Germany) to measure the absorption spectra. Single sides of six sheets of the cover glass were coated with the ZnO nanoparticle solution and heated at 150 °C on a hotplate for 20 min to form ZnO seed layers. They were immersed in the ZnO precursor solution and heated at 95 °C for 10 h while refreshing the precursor solution every 2.5 h in a convection oven. After the synthesis of ZnO nanowires, five samples were dipped into the $TiO_2$ precursor solutions for 10, 20, 40, 60, and 120 min to obtain ZnO–$TiO_2$ composites with various Zn/Ti ratios. A UV–vis–near-infrared spectrophotometer (V-570, Jasco Inc.) was utilized to measure the absorption spectra of seven samples (reference cover glass, ZnO nanowire, and five ZnO–$TiO_2$ composites on the cover glass substrates). The absorption spectra of cover glass were subtracted to remove the substrate effect.

**Measurement of Sensor Response to Ultraviolet (UV) and Ambient Light Sources.** The electrical characterization of devices was carried out using a potentiostat/galvanostat (CHI600D, CH Instruments Inc.). A UV lamp with a peak wavelength of $\lambda$ = 365 nm (LF206LS, UVitec Cambridge, U.K.) and an ambient light-emitting diode with the color rendering index of 94 and color temperature of 5500 K (NL200, HAREX, South Korea) were employed as UV and ambient light sources. DC bias values of 0.5 and 5 V were applied to ZnO nanowire and $TiO_2$ nanotube devices, respectively, and the currents through the nanomaterials were measured under various light intensities.

**Bending Test.** The bending tests of the ZnO nanowire and $TiO_2$ nanotube devices on a flexible PI substrate were conducted using a custom-made bending system consisting of a linear stage and a carrier film (polyester film with 0.5 mm thickness). The light sensors were attached on the carrier film, whose ends were connected to the linear


DOI: 10.1021/acs.langmuir.7b02332
Langmuir 2018, 34, 4132–4141

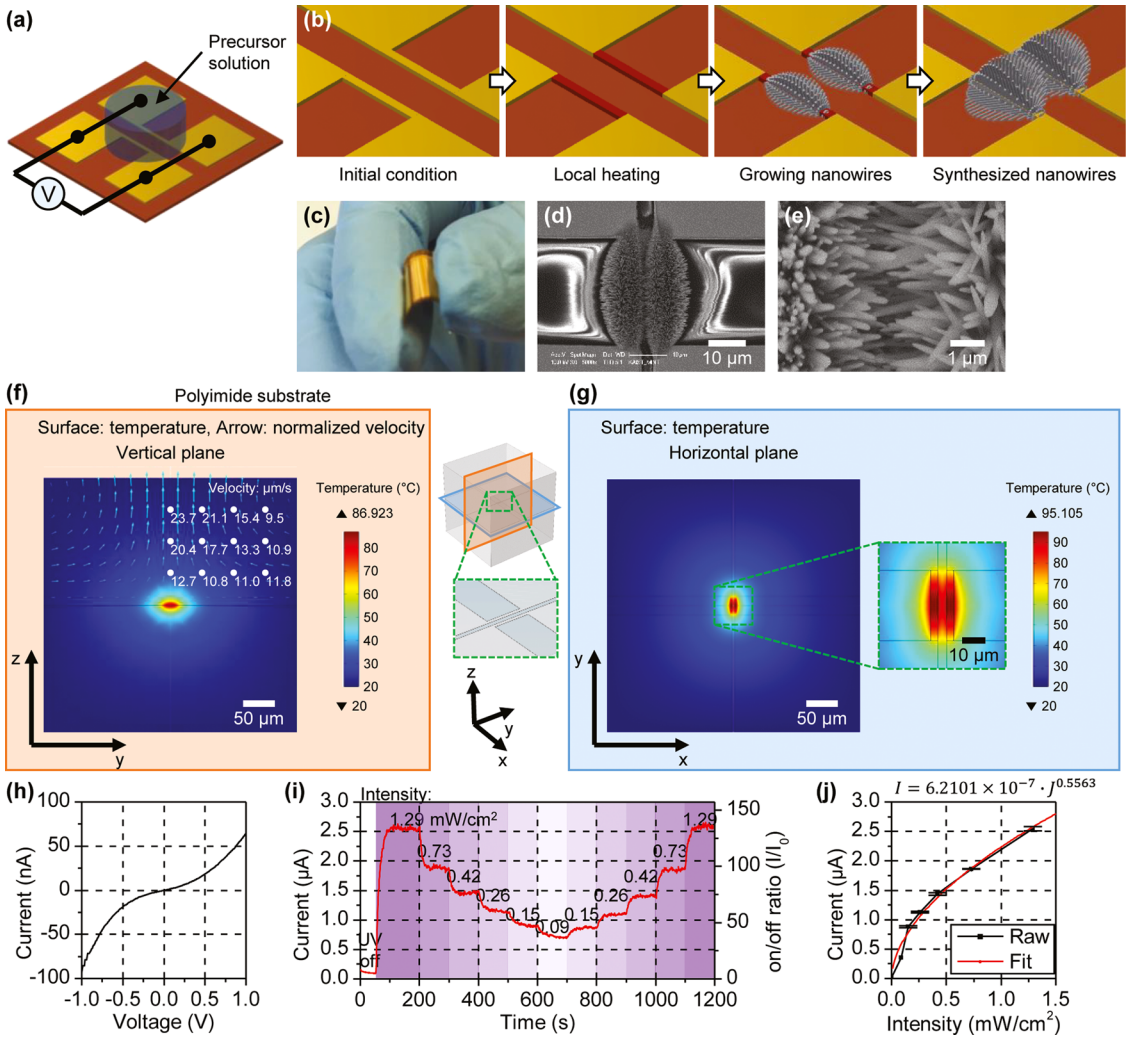


**Figure 2.** (a) Schematic of the experimental setup and (b) process flow for ZnO nanowire synthesis by the localized hydrothermal reaction; (c) photo and (d, e) SEM images of locally synthesized ZnO nanowires on a flexible substrate; (f) temperature and flow distribution in the precursor solution and PI substrate during the local hydrothermal synthesis process and (g) temperature profile on the surface of the microheater platform on the PI substrate; and (h) current−voltage ($I$−$V$) curve, (i) UV light sensing responses, and (j) current on/off ratio vs illuminance of the fabricated ZnO nanowire sensor.

stage. The film was bent with various radii of curvature by moving the linear stage.

## RESULTS AND DISCUSSION

The fabrication of the ZnO nanowire-based UV sensor relies on the localized hydrothermal reaction. The microheaters designed to generate highly localized heating were fabricated using photolithography and metal deposition processes. As shown in Figure S1a, a pair of microheaters with a length of 30 $\mu$m, a width of 3 $\mu$m, a thickness of 200 nm, and a gap of 4 $\mu$m was located at the center of device. The most important factor for local hydrothermal synthesis is the temperature localization. The numerical simulation result indicates that the thermal power density (power per unit area) is 308 000 times larger in the microheater than in the contact pads during Joule heating due to the large electrical resistance of the microheater (see Figure S1b in the Supporting Information). This concentrated heat generation enables a localized endothermal chemical reaction in the liquid precursor environment.

Figure 2a,b shows the schematic of the synthesis process for ZnO nanowires using the localized hydrothermal reaction. The synthesis mechanism is the same as that for general hydrothermal synthesis of ZnO nanowires, except for the localized reaction driven by Joule heating.[35] The solubility of ZnO in the precursor decreases at a higher temperature and therefore ZnO nanowires are synthesized by an endothermic chemical reaction.[37] The ZnO nanowire bundles grown from two neighboring microheaters become longer and eventually form an interconnection with each other. Figures 2c−e and S3a,b show the photo and scanning electron microscopy (SEM) images of locally synthesized ZnO nanowires on the PI substrate. The ZnO nanowires can be synthesized on the flexible polymer substrate because of the low seeding (150 °C) and synthesis (~95 °C) temperatures and nonharsh chemicals used for the liquid-phase reaction. Crystalline ZnO nanoparticles with an average diameter of 3 nm were used as seeds,[36] and the seed layer did not show any electrical current because of the electrical disconnection between the particles (see Figure S4 in the Supporting Information). The average diameter and length of ZnO nanowires were 200 nm and 4 $\mu$m, respectively. As shown in the cross-sectional SEM images of ZnO in Figure S2a,b, ZnO nanowires were directly synthesized on the surface



DOI: 10.1021/acs.langmuir.7b02332
Langmuir 2018, 34, 4132−4141

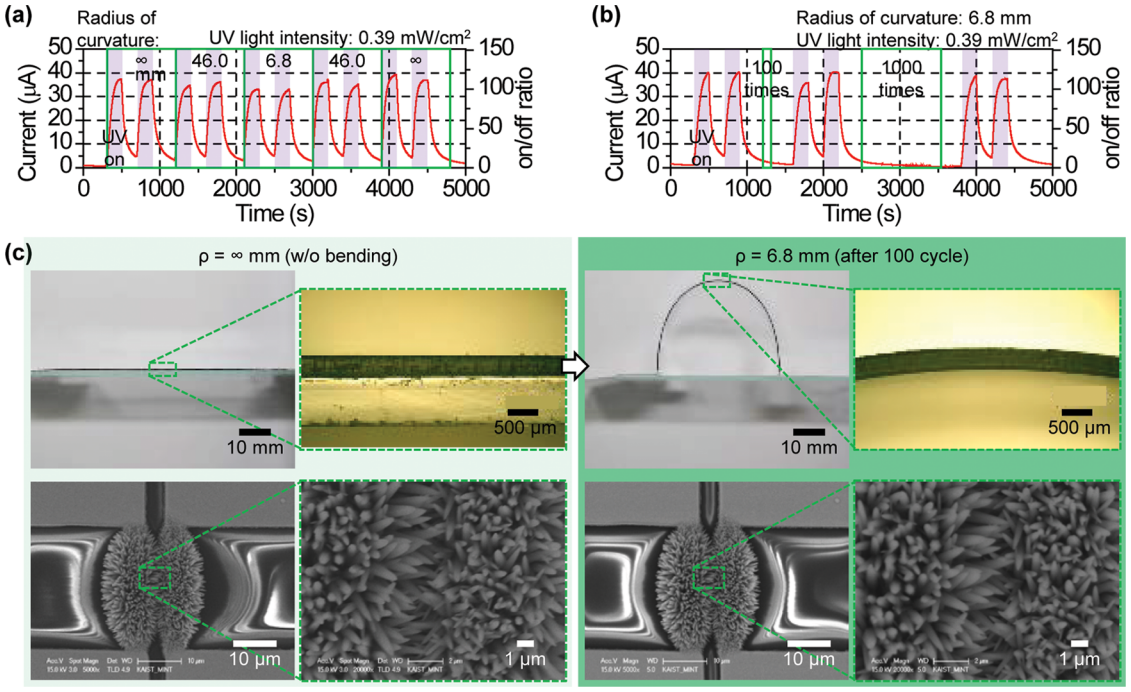


**Figure 3.** (a) UV light sensing response under various radii of curvature ($\rho$ = ∞ − 6.8 mm) and (b) repeated bending cycles ($\rho$ = 6.8 mm). (c) Optical and SEM images of the ZnO nanowire device under various radii of curvature ($\rho$ = ∞, 71.9, 46.0, 26.1, 16.6, and 6.8 mm). There are no notable deformations or cracks in the ZnO nanowires.

of the gold electrode, which enabled a close connection between nanowires and the electrode. Two ZnO nanowire bundles were connected with each other at the center of two microheaters in the form of a bridge, which can be used as the electrical path for the UV sensor.

The synthesis processes were analyzed by finite element method simulation of Joule heating and convective heat/mass transfers. The numerical simulation was conducted by COMSOL Multiphysics with "electric current" and "non-isothermal flow" modules. As shown in Figure S3a, a DC bias was applied to the microheater and heat generation was calculated by the electric current module. The calculated heat was applied to the heat source in the nonisothermal flow module, from which the temperature profile and flow of precursor solution were calculated. A local hot spot (maximum temperature = 95.1 °C) was generated at the microheaters, and this nonuniform temperature caused a convective flow of the precursor solution (Figure 2f,g). To verify the thermal insulation effect of the PI substrate, we conducted the same numerical simulation with a silicon (Si) substrate with a sufficiently thick (5 $\mu$m) insulation layer. Figure S3b,c shows the temperature profile and flow motion of the precursor solution on the $SiO_2$/Si substrate. Even though the same electrical bias was applied and the same amount of heat was generated, the temperature at the microheater only rose by 27.1 °C from the initial temperature (20 °C). This is because the thermal conductivity of PI (0.18 W/(m·K) at 300 K)[38] is 800 times lower than that of Si (142.2 W/(m·K))[39] and 6 times lower than that of $SiO_2$ (1.063 W/(m·K)[40] at 300 K). As a result, PI could effectively isolate thermal energy and thus generated higher local temperature even by consuming lower energy. Therefore, the use of polymer substrate not only widens the flexible device applications but also helps reduction of energy consumption during the synthesis and possible side effects (e.g., electrodeposition[41] and electrolysis[42]) originating from the high electrical bias applied in the liquid environment.

The current−voltage ($I$−$V$) curve of ZnO nanowires verified that nanowires were successfully synthesized on the electrodes and formed an electrical interconnection between electrodes (Figure 2h). Because the work function of ZnO (4.5 eV)[43] is lower than that of gold electrode,[44] the $I$−$V$ curve shows a Schottky contact behavior.[45−47] The band gap energy of ZnO is 3.37 eV that corresponds to a wavelength of 365 nm.[21] Thus, ZnO can show responses to different intensities of UV light by photoconductive effect, which is related to the electron−hole pair generation and chemisorption/desorption of oxygen on the surface of the sensing materials.[48] In the dark state, oxygen molecules are chemisorbed on the ZnO surface as $O_2^-$ ions by capturing free electrons from ZnO, and this generates a depletion layer near the surface.[49,50] When semiconductor materials absorb photon energy above their band gap, pairs of electrons and holes are generated. The holes generated by photons combine with chemisorbed oxygen ions existing on the surface of ZnO. The oxygen ions are converted to oxygen molecules ($O_2$) and then migrate from the surface of ZnO. In this process, free electrons are returned back to ZnO and function as mobile charge carriers. Furthermore, the electrons generated by photons also contribute to the electrical current as mobile charge carriers. Consequently, the concentration of mobile charge carriers is increased and the width of depletion layer is decreased.[49] Because of this surface reaction mechanism and high surface-to-volume ratio, one-dimensional nanomaterials such as nanowires and nanotubes provide much higher sensitivity and response speed than those of the bulk materials.[51,52] Figure 2i shows the real-time response of the ZnO nanowire sensor to the UV light with various intensities. The dark current of 19.1 nA was amplified to 2.54 $\mu$A under the light intensity of 1.29 mW/cm$^2$ with 19.4 s of rise time ($\tau_{r,90\%}$) and 16.7 s of decay time ($\tau_{d,10\%}$). The current through the ZnO



DOI: 10.1021/acs.langmuir.7b02332
Langmuir 2018, 34, 4132−4141

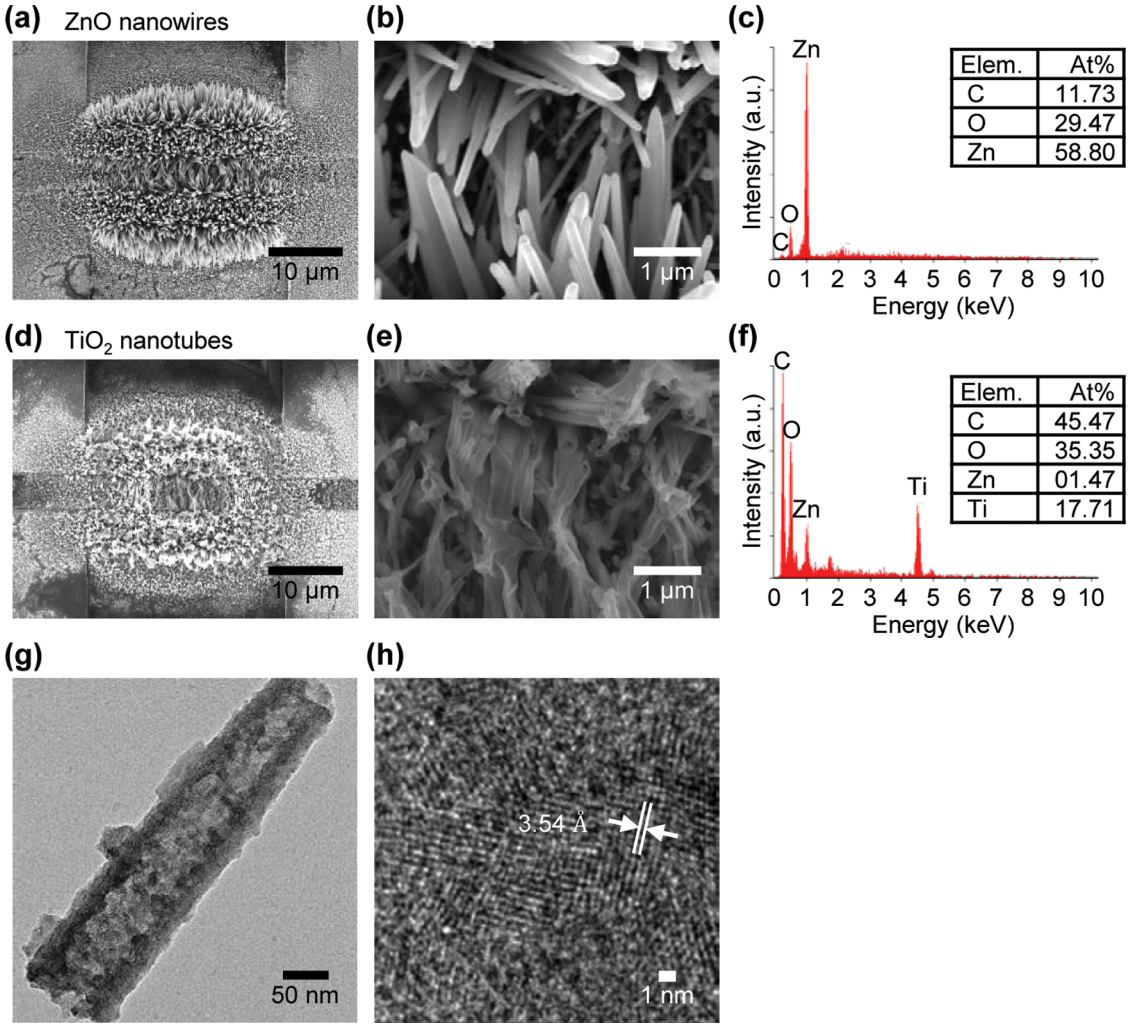


**Figure 4.** Microstructure and elemental characterization of synthesized ZnO nanowires and $TiO_2$ nanotubes: (a, b) SEM images and (c) EDS data of ZnO nanowires; (d, e) SEM images, (f) EDS data, and (g, h) TEM image of $TiO_2$ nanotubes.

nanowire interconnection exhibited an incremental change by stepwise change of UV light intensities. As shown in Figure 2j, the relationship between photocurrent and UV intensity obeys a power law,[48,53] $I = \alpha \times J^n$, where $I$ is the photocurrent ($\mu$A), $J$ is the intensity of UV light (mW/cm$^2$), and $\alpha$ ($6.2101 \times 10^{-7}$) and $n$ (0.5563) are coefficients.

To use the flexible sensors in practical applications, the devices must be robust under mechanical stresses. The mechanical robustness and UV light sensing characteristics of the flexible ZnO nanowire sensor device were tested in bending conditions. The device was initially in a flat condition but bent to various curvature radii ($\rho$ = 46.0 and 6.8 mm) while UV lamp was turned off and on with an intensity of 0.39 mW/cm$^2$. As shown in Figure 3a, the average on/off ratios ($I_{on}/I_{off}$) are 113.1, 107.5, 100.7, 107.6, and 116.0 in a flat condition, in bent conditions with curvature radii of 46.0, 6.8, and 46.0 mm, and back in a flat condition, respectively. Figure 3b shows the response after 100 and 1000 cycles of bending with a curvature radius of 6.8 mm. The average on/off ratio before bending and after 100 and 1000 cycles of bending were 122.6, 115.5, and 115.7, respectively. The sensing performance was maintained with little degradation by bending condition with various radii of curvature and repeated bending cycles. Figures 3c and S5 show the shapes of the ZnO nanowire network in a flat condition and under various curvature radii of 71.9, 46.0, 26.1, 16.6, and 6.8 mm. In these images, no destruction or damages can be found in the nanowire network by bending. In addition, the ZnO nanowire junction withstand with no observable changes after 1000 cycles of repeated bending with a curvature radius of 6.8 mm. We have also conducted the bending test along the transverse direction to the microheaters. Similar to the bending in the longitudinal direction, the electrical current fluctuated within 10% during the sequential bending down to a curvature radius of 6.8 mm (see Figure S6 in the Supporting Information).

These results indicate strong mechanical stability of ZnO nanowire junctions and robust bonding between synthesized ZnO nanowires and the metal electrode. These excellent mechanical characteristics can be attributed to the direct synthesis on the substrate and vertically grown structures of the nanowire array. The nanowires were directly synthesized from the nucleation points on the surface of the electrode by forming crystallized structures, thereby providing stronger bonding to the electrode than that from the van der Waals or electrostatic forces that exist between the electrodes and ex situ grown, subsequently assembled nanostructures (i.e., nanostructures assembled on the electrodes by conventional integration methods such as drop casting, dielectrophoresis, or micro-



DOI: 10.1021/acs.langmuir.7b02332
Langmuir 2018, 34, 4132−4141

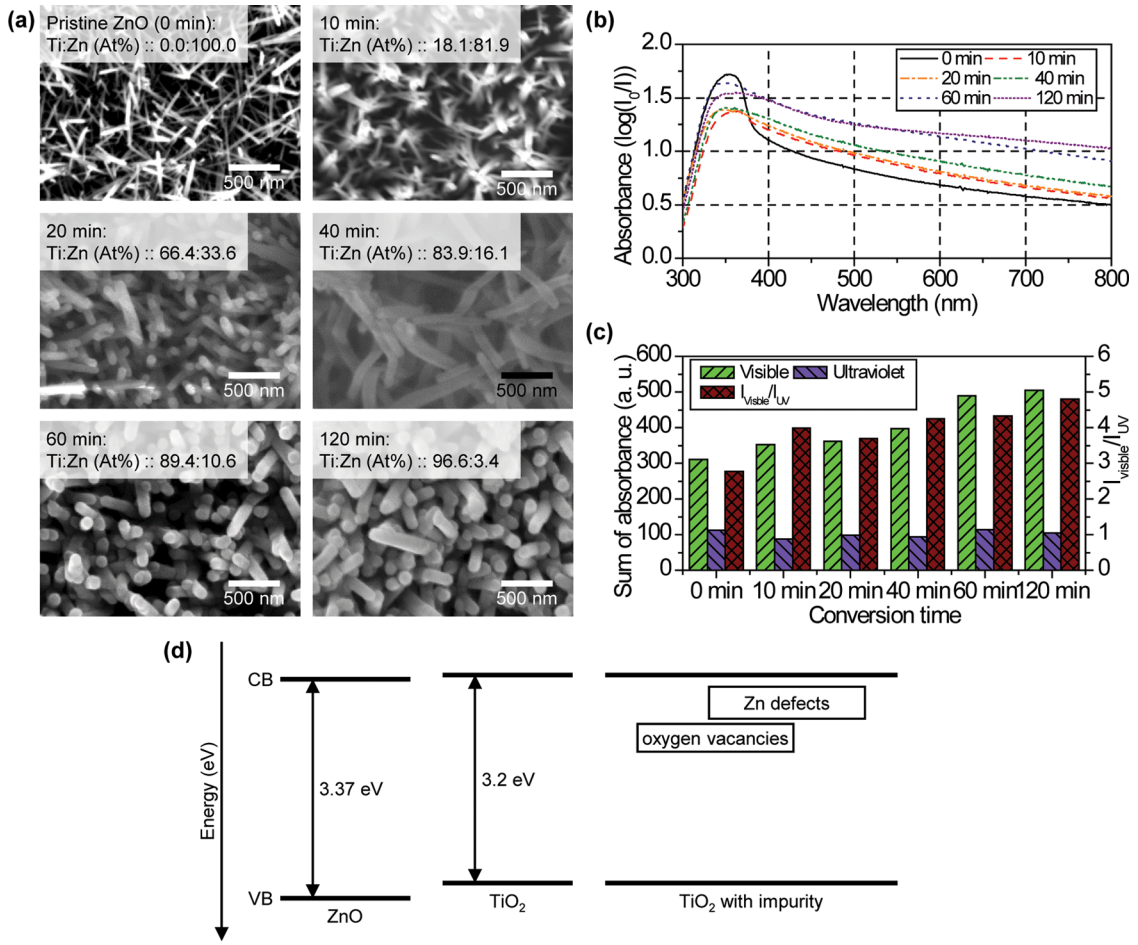


**Figure 5.** (a) Microstructural change of ZnO−$TiO_2$ composites after different conversion periods. The diameter of the nanomaterials and atomic ratios of Ti/Zn increase after conversion for longer periods. (b) Absorption spectra and (c) absorbance ratio of visible (380−820 nm) to UV (<380 nm) light region of ZnO−$TiO_2$ composites. The absorbance of visible light region is increased by increasing the concentration of Ti. (d) Energy band diagram of $TiO_2$ containing oxygen vacancies and Zn defects.

contact printing). As mentioned above, another reason for the mechanical robustness of ZnO nanowires is the vertically grown structure with respect to the substrate. Because we have fabricated a small-sized sensor, the amount of absolute deformation is very small. However, the strain is the same regardless of the size of the structure under the same curvature radius. Under bending conditions, three-dimensional bridging structures fabricated in this work are effective in reducing stress. As shown in Figure S7a,b, the bending stress in nanowires is proportional to the angle of bending and inversely proportional to the length of nanowire if pure bending condition is assumed. Under the same bending condition, vertically grown nanowires provide a larger root-to-junction length and thus reduce bending stresses as compared to those in horizontally grown nanowires (see Section 7 in the Supporting Information).[54]

Not only ZnO nanowires but also $TiO_2$ nanotubes can be used as light sensors because of their wide band gap (anatase 3.2 eV, rutile 3.0 eV).[55] The synthesis method of $TiO_2$ nanotubes is also based on the localized wet chemical reactions.[55] This method consists of two steps: localized hydrothermal reaction for the synthesis of ZnO nanowires and liquid phase deposition (LPD) of $TiO_2$ nanotubes using ZnO nanowires as templates. As shown in Figure 1, presynthesized ZnO nanowires are used as templates for the reaction in the $TiO_2$ precursor solution. The synthesis mechanism of $TiO_2$ nanotubes via the LPD method consists of two parallel reactions: $TiO_2$ deposition and ZnO etching. $TiO_2$ is deposited on the surface of ZnO nanowires by the hydrolysis reaction of the titanium-fluoro complex ion ($TiF_6^{2-}$) from ammonium hexafluorotitanate. This reaction generates fluoride ($F^-$) ions that are combined with boric acid and accelerate the hydrolysis reactions.[56,57] The ZnO nanowires are coated with the $TiO_2$ nanofilm, and the $TiO_2$/ZnO core−sheath nanostructures are acquired. Simultaneously, the ZnO nanowire templates are etched by the acidic precursor solution.[58] Figure 4a−f shows the SEM images and energy-dispersive spectrometry (EDS) data of presynthesized ZnO nanowires and $TiO_2$ nanotubes converted from the ZnO nanowire template. It can be observed that the shapes of ZnO nanowire templates are maintained in the $TiO_2$ nanotube bundle. However, the outer diameters of the $TiO_2$ nanotubes are several tens of nanometers thicker than those of the ZnO nanowires because of the thickness of the deposited $TiO_2$ nanotube film. Figure S2c,d shows the cross-sectional SEM image of the $TiO_2$ nanotube device. Slightly rough structures were formed during the conversion process, which indicates that the $TiO_2$ precursor reached the roots of the ZnO nanowire bundle and ZnO nanowires were converted into $TiO_2$ nanotubes. The image shows a close connection between the $TiO_2$ nanotube and the Au electrode. As shown in the transmission electron microscopy (TEM) image of the


DOI: 10.1021/acs.langmuir.7b02332
Langmuir 2018, 34, 4132−4141

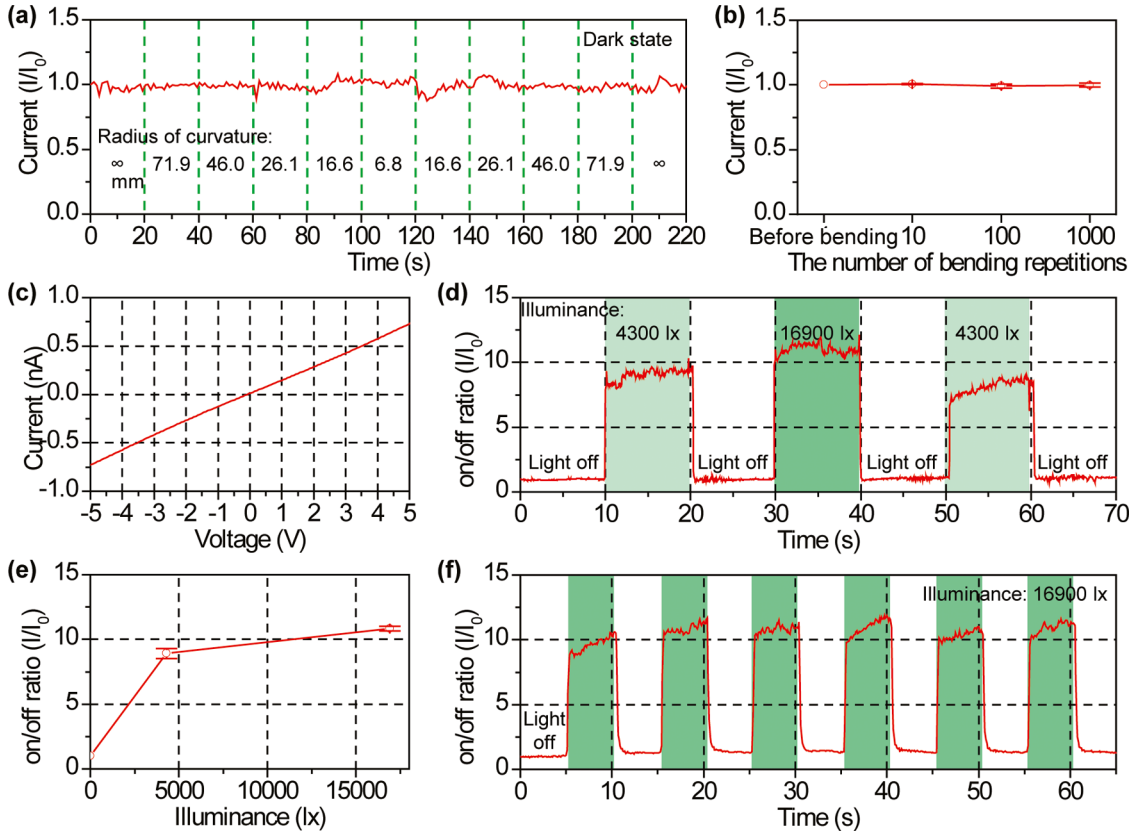


**Figure 6.** (a) Current through the $TiO_2$ nanotube device under various radii of curvature ($\rho$ = ∞, 71.9, 46.0, 26.1, 16.6, and 6.8 mm) and (b) after repeated bending cycles ($\rho$ = 6.8 mm). (c) Current−voltage curve of the $TiO_2$ nanotube device. (d) Responses of the $TiO_2$ nanotube sensor to various illuminance of ambient light. (e) Current on/off ratio vs illuminance curve. (f) Dynamic response under rapid turn-on and turn-off cycles of ambient light.

$TiO_2$ nanotube (Figure 4g) and EDS data (Figure 4f), $TiO_2$ nanotubes show an obvious tubular nanostructure with a Ti/Zn ratio of 0.923:0.077. These results indicate that the ZnO nanowires were mostly removed during the conversion process but small amount of Zn still remained after the reaction. The high resolution TEM image shows that the material is a mixture of mostly polycrystalline and partially amorphous crystalline structures (Figure 4h). The lattice spacing of the crystallized region is 3.54 Å that corresponds to the (101) plane of the typical anatase $TiO_2$.[59]

$TiO_2$ materials are typically used for UV light sensors because of their band gap corresponding to the wavelength of UV light (e.g., band gap of anatase $TiO_2$ = 3.2 eV).[54] However, their photoelectric properties can be tuned by introducing Zn impurities to realize ambient light sensors.[60−62] In our process, a small amount of Zn remained after the synthesis of $TiO_2$ nanotubes as explained above, thereby Zn impurity within $TiO_2$ nanotubes is realized without requiring further doping process. To analyze the photonic characteristics of ZnO and ZnO−$TiO_2$ composites, their absorption spectra were measured. As shown in Figure 5a, six samples with different atomic ratios of Ti/Zn from 0:100 to 97:3 were prepared by increasing the conversion time on the glass substrate. Figure 5b,c shows the absorption spectra and absorbance ratio of the visible (380−820 nm) to UV (<380 nm) light region for the ZnO nanowire and $TiO_2$ nanotube samples. The absorbance in the UV region did not show significant change, whereas that in the visible region was gradually increased by 13, 16, 28, 58, and 63% for the samples with Ti atomic concentrations of 18.1, 66.4, 83.9, 89.4, and 96.6%, respectively, than for the pristine ZnO nanowires. Therefore, the absorbance ratio of the visible-to-UV region ($I_{visible}/I_{UV}$) was increased with the increasing Ti-to-Zn ratio. Zn atoms and oxygen vacancies could not be perfectly removed inside the $TiO_2$ nanotubes by the LPD method. However, these impurities can be helpful in increasing the absorption of visible light in the $TiO_2$ nanotubes. The oxygen vacancy states are located between the valence and conduction bands of $TiO_2$, locating at 2.02−2.45 eV above the valence band, which corresponds to a wavelength of 506−614 nm.[60,61] In addition, the Zn-related defects in the $TiO_2$ nanotubes contribute to the absorption in the wavelength of 410−490 nm.[61] In summary, Zn defects generate intermediate band gap levels between valance and conduction bands and thus reduce energies required to excite electrons to the conduction band (Figure 5d).

To verify the mechanical robustness of the $TiO_2$ nanotube device, it was bent to a curvature radius of 6.8 mm and recovered to a flat condition while measuring the electrical current. As shown in Figure 6a, the current was stable during static bending with different curvature radii. Figure 6b shows the current through the $TiO_2$ nanotube device after 10, 100, and 1000 bending cycles. There was only 2% current drop after 1000 times of repeated bending, which indicates no damage or deformation in the $TiO_2$ nanotube device during repeated bending.

The resistance of the $TiO_2$ nanotube sensor was measured under various illuminance of ambient light. The sensing mechanism of the $TiO_2$ nanotube sensors is similar to that of


DOI: 10.1021/acs.langmuir.7b02332
Langmuir 2018, 34, 4132−4141

the ZnO nanowire sensors. Upon exposure to ambient light, the electron−hole pairs are generated and surface-adsorbed oxygen ions are converted into $O_2$ molecules and then desorbed from the surface of $TiO_2$ nanotubes.[63,64] The $I-V$ curve shown in Figure 6c indicates very weak Schottky contact between $TiO_2$ nanotube bundles and electrodes under the dark state. Generally, the contact between $TiO_2$ and gold shows a Schottky behavior because the work function of $TiO_2$[65] is lower than that of gold.[43] However, in this work, the Zn impurities and oxygen vacancies filled the band gap of $TiO_2$ and Fermi level was adjusted as a consequence. Figure 6d shows the real-time response of the $TiO_2$ nanotube sensor to the ambient light. The dark current of 62.9 pA was amplified by 8.92 and 10.82 times under 4300 and 16 900 lx of ambient light. The current passing through $TiO_2$ nanotubes was increased by higher illuminance of ambient light (Figure 6e). As shown in Figure 6f, the $TiO_2$ nanotube exhibits a rapid response to turn-on and turn-off cycles under 16 900 lx ambient light. The rise time ($\tau_{r,90\%}$) and decay time ($\tau_{d,10\%}$) are 0.16 and 0.35 s, respectively. The hollow structures of $TiO_2$ nanotubes shorten the electron path to the surface of nanostructures, which reduces the recombination probability.[66,67] A large number of electrons can quickly reach the oxygen molecules, and this reduces the rise time and decay time.

## CONCLUSIONS

We have developed a ZnO nanowire-based UV light sensor and a $TiO_2$ nanotube-based ambient light sensor on flexible substrates using localized hydrothermal synthesis of ZnO nanowires and liquid phase deposition of $TiO_2$ thin films on the ZnO nanowire templates. The ZnO nanowire and $TiO_2$ nanotube sensors exhibited sensitive and rapid sensing response to UV and ambient light, respectively. Moreover, the devices showed reliable light sensing performance under mechanical stress because of the robust connection between nanowires and electrodes resulting from the direct synthesis process. They would be very useful for the sensors in wearable and internet of things applications because of their simple and low-cost fabrication methods, ultracompact form factors, mechanical robustness, and ultralow power consumption.

## ASSOCIATED CONTENT

### Supporting Information

The Supporting Information is available free of charge on the ACS Publications website at DOI: 10.1021/acs.langmuir.7b02332.

Details of the microheater device; additional SEM images of ZnO nanowires and $TiO_2$ nanotubes; numerical simulation of the local hydrothermal synthesis method; electrical connection by the seed layer; shape of ZnO nanowires under bending condition; ZnO nanowire bending test along the transverse direction to the microheaters; deformation of nanowires under bending condition; comparison of light sensing performance (PDF)

## AUTHOR INFORMATION


### Corresponding Author

*E-mail: inkyu@kaist.ac.kr.

### ORCID

Daejong Yang: 0000-0002-8774-5843

Inkyu Park: 0000-0001-5761-7739


### Author Contributions

The manuscript was written through contributions of all authors. All authors have given approval to the final version of the manuscript.

### Notes

The authors declare no competing financial interest.

## ACKNOWLEDGMENTS

This research was supported by Basic Science Research Programs (No. 2015R1A5A1037668) through the National Research Foundation (NRF) funded by the Korean government. This research was also supported by Multi-Ministry Collaborative R&D Program (Development of Techniques for Identification and Analysis of Gas Molecules to Protect Against Toxic Substances) through the National Research Foundation of Korea (NRF) funded by KNPA, MSIT, MOTIE, ME, NFA (NRF-2017M3D9A1073858).

## REFERENCES


(1) Xiang, J.; Lu, W.; Hu, Y.; Wu, Y.; Yan, H.; Lieber, C. M. Ge/Si Nanowire Heterostructures as High-Performance Field-Effect Transistors. *Nature* **2006**, *441*, 489−493.

(2) Im, J.-H.; Luo, J.; Franckevicius, M.; Pellet, N.; Gao, P.; Moehl, T.; Zakeeruddin, S. M.; Nazeeruddin, M. K.; Gratzel, M.; Park, N.-G. Nanowire Perovskite Solar Cell. *Nano Lett.* **2015**, *15*, 2120−2126.

(3) Xu, S.; Qin, Y.; Xu, C.; Wei, Y.; Yang, R.; Wang, Z. L. Self-Powered Nanowire Devices. *Nat. Nanotechnol.* **2010**, *5*, 366−373.

(4) Xia, X.; Tu, J.; Zhang, Y.; Wang, X.; Gu, C.; Zhao, X.-B.; Fan, H. J. High-Quality Metal Oxide Core/Shell Nanowire Arrays on Conductive Substrates for Electrochemical Energy Storage. *ACS Nano* **2012**, *6*, 5531−5538.

(5) Zeng, H.; Xu, X.; Bando, Y.; Gautam, U. K.; Zhai, T.; Fang, X.; Liu, B.; Golberg, D. Template Deformation-Tailored ZnO Nanorod/Nanowire Arrays: Full Growth Control and Optimization of Field-Emission. *Adv. Funct. Mater.* **2009**, *19*, 3165−3172.

(6) Yang, D.; Kang, K.; Kim, D.; Li, Z.; Park, I. Fabrication of Heterogeneous Nanomaterial Array by Programmable Heating and Chemical Supply within Microfluidic Platform Towards Multiplexed Gas Sensing Application. *Sci. Rep.* **2015**, *5*, No. 8149.

(7) Fu, X.-W.; Liao, Z.-M.; Zhou, Y.-B.; Wu, H.-C.; Bie, Y.-Q.; Xu, J.; Yu, D.-P. Graphene/ZnO Nanowire/Graphene Vertical Structure Based Fast-Response Ultraviolet Photodetector. *Appl. Phys. Lett.* **2012**, *100*, No. 223114.

(8) Yang, D.; Cho, H.; Koo, S.; Vaidyanathan, S. R.; Woo, K.; Yoon, Y.; Choo, H. Simple, Large-Scale Fabrication of Uniform Raman-Enhancing Substrate with Enhancement Saturation. *ACS Appl. Mater. Interfaces* **2017**, *9*, 19092−19101.

(9) Athauda, T. J.; Hari, P.; Ozer, R. R. Tuning Physical and Optical Properties of ZnO Nanowire Arrays Grown on Cotton Fibers. *ACS Appl. Mater. Interfaces* **2013**, *5*, 6237−6246.

(10) Liu, J.; Wu, W.; Bai, S.; Qin, Y. Synthesis of High Crystallinity ZnO Nanowire Array on Polymer Substrate and Flexible Fiber-Based Sensor. *ACS Appl. Mater. Interfaces* **2011**, *3*, 4197−4200.

(11) Prouzet, E.; Ravaine, S.; Sanchez, C.; Backov, R. Bio-Inspired Synthetic Pathways and Beyond: Integrative Chemistry. *New J. Chem.* **2008**, *32*, 1284−1299.

(12) Kolmakov, A.; Moskovits, M. Chemical Sensing and Catalysis by One-Dimensional Metal-Oxide Nanostructures. *Annu. Rev. Mater. Res.* **2004**, *34*, 151−180.

(13) Yu, H.; Li, J.; Loomis, R. A.; Wang, L.-W.; Buhro, W. E. Two-Versus Three-Dimensional Quantum Confinement in Indium Phosphide Wires and Dots. *Nat. Mater.* **2003**, *2*, 517−520.

(14) Huang, X.; Zhao, Z.; Chen, Y.; Chiu, C.-Y.; Ruan, L.; Liu, Y.; Li, M.; Duan, X.; Huang, Y. High Density Catalytic Hot Spots in Ultrafine Wavy Nanowires. *Nano Lett.* **2014**, *14*, 3887−3894.




DOI: 10.1021/acs.langmuir.7b02332
*Langmuir* 2018, 34, 4132−4141

(15) Wang, C.; Yin, L.; Zhang, L.; Xiang, D.; Gao, R. Metal Oxide Gas Sensors: Sensitivity and Influencing Factors. *Sensors* **2010**, *10*, 2088−2106.
(16) Yang, J.; Hidajat, K.; Kawi, S. Synthesis of Nano-$SnO_2$/SBA-15 Composite as a Highly Sensitive Semiconductor Oxide Gas Sensor. *Mater. Lett.* **2008**, *62*, 1441−1443.
(17) Cui, Y.; Wei, Q. Q.; Park, H. K.; Lieber, C. M. Nanowire Nanosensors for Highly Sensitive and Selective Detection of Biological and Chemical Species. *Science* **2001**, *293*, 1289−1292.
(18) Yang, D.; Fuadi, M. K.; Kang, K.; Kim, D.; Li, Z.; Park, I. Multiplexed Gas Sensor Based on Heterogeneous Metal Oxide Nanomaterial Array Enabled by Localized Liquid-Phase Reaction. *ACS Appl. Mater. Interfaces* **2015**, *7*, 10152−10161.
(19) Kim, J.; Kwon, S.; Park, J.-K.; Park, I. Quantum Dot-Based Immunoassay Enhanced by High-Density Vertical ZnO Nanowire Array. *Biosens. Bioelectron.* **2014**, *55*, 209−215.
(20) Tang, Z. K.; Wong, G. K. L.; Yu, P.; Kawasaki, M.; Ohtomo, A.; Koinuma, H.; Segawa, Y. Room-Temperature Ultraviolet Laser Emission from Self-Assembled ZnO Microcrystallite Thin Films. *Appl. Phys. Lett.* **1998**, *72*, 3270−3272.
(21) Bai, S.; Wu, W.; Qin, Y.; Cui, N.; Bayerl, D. J.; Wang, X. High-Performance Integrated ZnO Nanowire UV Sensors on Rigid and Flexible Substrates. *Adv. Funct. Mater.* **2011**, *21*, 4464−4469.
(22) Alenezi, M. R.; Henley, S. J.; Silva, S. R. P. On-chip Fabrication of High Performance Nanostructured ZnO UV Detectors. *Sci. Rep.* **2015**, *5*, No. 8516.
(23) Wan, Q.; Li, Q. H.; Chen, Y. J.; Wang, T. H.; He, X. L.; Li, J. P.; Lin, C. L. Fabrication and ethanol sensing characteristics of ZnO nanowire gas sensors. *Appl. Phys. Lett.* **2004**, *84*, 3654−3656.
(24) Chávez, F.; Pérez-Sánchez, G. F.; Goiz, O.; Zaca-Morán, P.; Peña-Sierra, R.; Morales-Acevedo, A.; Felipec, C.; Soledad-Priego, M. Sensing Performance of Palladium-Functionalized $WO_3$ Nanowires by a Drop-Casting Method. *Appl. Surf. Sci.* **2013**, *275*, 28−35.
(25) Fiorido, T.; Bendahan, M.; Aguir, K.; Bernardini, S.; Martini, C.; Brisset, H.; Fages, F.; Videlot-Ackermannc, C.; Ackermann, J. All Solution Processed Flexible Ammonia Gas and Light Sensors Based on $\alpha,\omega$-Hexyl-Distyrylbithiophene Films. *Sens. Actuators, B* **2010**, *151*, 77−82.
(26) Xie, C.; Xiao, L.; Hu, M.; Bai, Z.; Xia, X.; Zeng, D. Fabrication and Formaldehyde Gas-Sensing Property of ZnO-$MnO_2$ Coplanar Gas Sensor Arrays. *Sens. Actuators, B* **2010**, *145*, 457−463.
(27) Ul Hasan, K.; Nur, O.; Willander, M. Screen Printed ZnO Ultraviolet Photoconductive Sensor on Pencil Drawn Circuitry Over Paper. *Appl. Phys. Lett.* **2012**, *100*, No. 211104.
(28) Li, B.; Santhanam, S.; Schultz, L.; Jeffries-EL, M.; Iovu, M. C.; Sauvé, G.; Cooper, J.; Zhang, R.; Revelli, J. C.; Kusne, A. G.; et al. Inkjet Printed Chemical Sensor Array Based on Polythiophene Conductive Polymers. *Sens. Actuators, B* **2007**, *123*, 651−660.
(29) Hsieh, G.-W.; Wang, J.; Ogata, K.; Robertson, J.; Hofmann, S.; Milne, W. I. Stretched Contact Printing of One-Dimensional Nanostructures for Hybrid Inorganic-Organic Field Effect Transistors. *J. Phys. Chem. C* **2012**, *116*, 7118−7125.
(30) Yan, Z.; Jureller, J. E.; Sweet, J.; Guffey, M. J.; Pelton, M.; Scherer, N. F. Three-Dimensional Optical Trapping and Manipulation of Single Silver Nanowires. *Nano Lett.* **2012**, *12*, 5155−5161.
(31) Reynolds, K.; Komulainen, J.; Kivijakola, J.; Lovera, P.; Iacopino, D.; Pudas, M.; Vähäkangas, J.; Röning, J.; Redmond, G. Probe Based Manipulation and Assembly of Nanowires into Organized Meso-structures. *Nanotechnology* **2008**, *19*, No. 485301.
(32) Heo, K.; Cho, E.; Yang, J.-E.; Kim, M.-H.; Lee, M.; Lee, B. Y.; Kwon, S. G.; Lee, M.-S.; Jo, M.-H.; Choi, H.-J.; Hyeon, T.; Hong, S. Large-Scale Assembly of Silicon Nanowire Network-Based Devices Using Conventional Microfabrication Facilities. *Nano Lett.* **2008**, *8*, 4523−4527.
(33) Bellino, M. G.; Calvo, E. J.; Gordillo, G. J. Nanowire Manipulation on Surfaces Through Electrostatic Self-Assembly and Magnetic Interactions. *Phys. Status Solidi RRL* **2009**, *3*, 1−3.
(34) Leiterer, C.; Broenstrup, G.; Jahr, N.; Urban, M.; Arnold, C.; Christiansen, S.; Fritzsche, W. Applying Contact to Individual Silicon Nanowires Using a Dielectrophoresis (DEP)-Based Technique. *J. Nanopart. Res.* **2013**, *15*, No. 1628.
(35) Yang, D.; Kim, D.; Ko, S. H.; Pisano, A. P.; Li, Z.; Park, I. Focused Energy Field Method for the Localized Synthesis and Direct Integration of 1D Nanomaterials on Microelectronic Devices. *Adv. Mater.* **2015**, *27*, 1207−1215.
(36) Pacholski, C.; Kornowski, A.; Weller, H. Self-Assembly of ZnO: From Nanodots to Nanorods. *Angew. Chem., Int. Ed.* **2002**, *41*, 1188−1191.
(37) Li, Q.; Kumar, V.; Li, Y.; Zhang, H.; Marks, T. J.; Chang, R. P. H. Fabrication of ZnO Nanorods and Nanotubes in Aqueous Solutions. *Chem. Mater.* **2005**, *17*, 1001−1006.
(38) Rule, D. L.; Smith, D. R.; Sparks, L. L. Thermal Conductivity of Polypyromellitimide Film with Alumina Filler Particles from 4.2 to 300 K. *Cryogenics* **1996**, *36*, 283−290.
(39) Shanks, H. R.; Maycock, P. D.; Sidles, P. H.; Danielson, G. C. Thermal Conductivity of Silicon from 300 to 1400 °K. *Phys. Rev.* **1963**, *130*, 1743−1748.
(40) Chien, H.-C.; Yao, D.-J.; Huang, M.-J.; Chang, T.-Y. Thermal Conductivity Measurement and Interface Thermal Resistance Estimation Using $SiO_2$ Thin Film. *Rev. Sci. Instrum.* **2008**, *79*, No. 054902.
(41) Zumdahl, S. S.; Zumdahl, S. A. *Chemistry*, 7th ed.; Houghton Mifflin: Boston, 2007; pp 790−839.
(42) Kim, H.; Moon, J. Y.; Lee, H. S. Growth of ZnO Nanorods on Various Substrates by Electrodeposition. *Electron. Mater. Lett.* **2009**, *5*, 135−138.
(43) Jacobi, K.; Zwicker, G.; Gutmann, A. Work Function, Electron Affinity and Band Bending of Zinc Oxide Surfaces. *Surf. Sci.* **1984**, *141*, 109−125.
(44) Hansen, W. N.; Johnson, K. B. Work Function Measurements in Gas Ambient. *Surf. Sci.* **1994**, *316*, 373−382.
(45) Pierret, R. F. *Semiconductor Device Fundamentals*; Addison-Wesley: Boston, 1996 ; pp 477−504.
(46) Singh, N.; Yan, C.; Lee, P. S.; Comini, E. Sensing Properties of Different Classes of Gases Based on the Nanowire-Electrode Junction Barrier Modulation. *Nanoscale* **2011**, *3*, 1760−1765.
(47) Wei, T.-Y.; Yeh, P.-H.; Lu, S.-Y.; Wang, Z. L. Gigantic Enhancement in Sensitivity Using Schottky Contacted Nanowire Nanosensor. *J. Am. Chem. Soc.* **2009**, *131*, 17690−17695.
(48) Kind, H.; Yan, H.; Messer, B.; Law, M.; Yang, P. Nanowire Ultraviolet Photodetectors and Optical Switches. *Adv. Mater.* **2002**, *14*, 158−160.
(49) Lang, Y.; Gao, H.; Jiang, W.; Xu, L.; Hou, H. Photoresponse and Decay Mechanism of an Individual ZnO Nanowire UV Sensor. *Sens. Actuators, A* **2012**, *174*, 43−46.
(50) Yamazoe, N.; Fuchigami, J.; Kishikawa, M.; Seiyama, T. Interactions of Tin Oxide Surface with $O_2$, $H_2O$ and $H_2$. *Surf. Sci.* **1979**, *86*, 335−344.
(51) Liu, S.; Wang, Z.; Yu, C.; Wu, H. B.; Wang, G.; Dong, Q.; Qiu, J.; Eychmüller, A.; Lou, X. W. A Flexible $TiO_2$(B)-Based Battery Electrode with Superior Power Rate and Ultralong Cycle Life. *Adv. Mater.* **2013**, *25*, 3462−3467.
(52) Suehiro, J.; Nakagawa, N.; Hidaka, S.-I.; Ueda, M.; Imasaka, K.; Higashihata, M.; Okada, T.; Hara, M. Dielectrophoretic Fabrication and Characterization of a ZnO Nanowire-Based UV Photosensor. *Nanotechnology* **2006**, *17*, 2567−2573.
(53) Rose, A. *Concepts in Photoconductivity and Allied Problems*; Interscience Publishers: New York, 1963; pp 33−43.
(54) Beer, F.; Johnston, E. R., Jr.; DeWolf, J.; Mazurek, D. *Mechanics of Materials*, 6th ed.; McGraw-Hill: New York, 2011; pp 221−233.
(55) Tang, H.; Berger, H.; Schmid, P. E.; Lévy, F.; Burri, G. Photoluminescence in $TiO_2$ Anatase Single Crystals. *Solid State Commun.* **1993**, *87*, 847−850.
(56) Deki, S.; Aoi, Y.; Hiroi, O.; Kajinami, A. Titanium (IV) Oxide Thin Films Prepared from Aqueous Solution. *Chem. Lett.* **1996**, *25*, 433−434.


DOI: 10.1021/acs.langmuir.7b02332
*Langmuir* 2018, 34, 4132−4141

(57) Xu, C.; Shin, P. H.; Cao, L.; Wu, J.; Gao, D. Ordered $TiO_2$ Nanotube Arrays on Transparent Conductive Oxide for Dye-Sensitized Solar Cells. *Chem. Mater.* **2010**, *22*, 143−148.
(58) Lee, J.-H.; Leu, I.-C.; Hsu, M.-C.; Chung, Y.-W.; Hon, M.-H. Fabrication of Aligned $TiO_2$ One-Dimensional Nanostructured Arrays Using a One-Step Templating Solution Approach. *J. Phys. Chem. B* **2005**, *109*, 13056−13059.
(59) Wisitsoraat, A.; Tuantranont, A.; Comini, E.; Sberveglieri, G.; Wlodarski, W. Characterization of n-Type and p-Type Semiconductor Gas Sensors Based on $NiO_x$ Doped $TiO_2$ Thin Films. *Thin Solid Films* **2009**, *517*, 2775−2780.
(60) He, J.; Behera, R. K.; Finnis, M. W.; Li, X.; Dickey, E. C.; Phillpot, S. R.; Sinnott, S. B. Prediction of High-Temperature Point Defect Formation in $TiO_2$ from Combined Ab initio and Thermodynamic Calculations. *Acta Mater.* **2007**, *55*, 4325−4337.
(61) Nakamura, I.; Negishi, N.; Kutsuna, S.; Ihara, T.; Sugihara, S.; Takeuchi, K. Role of Oxygen Vacancy in the Plasma-Treated $TiO_2$ Photocatalyst with Visible Light Activity for NO Removal. *J. Mol. Catal. A: Chem.* **2000**, *161*, 205−212.
(62) Yang, L.; Zhang, Y.; Ruan, W.; Zhao, B.; Xu, W.; Lombardi, J. R. Improved Surface-Enhanced Raman Scattering Properties of $TiO_2$ Nanoparticles by Zn Dopant. *J. Raman Spectrosc.* **2010**, *41*, 721−726.
(63) Cao, C.; Hu, C.; Wang, X.; Wang, S.; Tian, Y.; Zhang, H. UV Sensor Based on $TiO_2$ Nanorod Arrays on FTO Thin Film. *Sens. Actuators, B* **2011**, *156*, 114−119.
(64) Xiao, P.; Liu, D.; Garcia, B. B.; Sepehri, S.; Zhang, Y.; Cao, G. Electrochemical and Photoelectrical Properties of Titania Nanotube Arrays Annealed in Different Gases. *Sens. Actuators, B* **2008**, *134*, 367−372.
(65) Smith, G. X. R.; Crook, R.; Wadhawan, J. D. Measuring the Work Function of $TiO_2$ Nanotubes Using Illuminated Electrostatic Force Microscopy. *J. Phys.: Conf. Ser.* **2013**, *471*, No. 012045.
(66) Paulose, M.; Varghese, O. K.; Mor, G. K.; Grimes, C. A.; Ong, K. G. Unprecedented Ultra-High Hydrogen Gas Sensitivity in Undoped Titania Nanotubes. *Nanotechnology* **2006**, *17*, 398−402.
(67) Mamat, M. H.; Ishak, N. I.; Khusaimi, Z.; Zahidi, M. M.; Abdullah, M. H.; Muhamad, S.; Sin, N. D. M.; Mahmood, M. R. Thickness-Dependent Characteristics of Aluminium-Doped Zinc Oxide Nanorod-Array-Based, Ultraviolet Photoconductive Sensors. *Jpn. J. Appl. Phys.* **2012**, *51*, No. 06FF03.



DOI: 10.1021/acs.langmuir.7b02332
*Langmuir* 2018, 34, 4132−4141